BIOCHEMISTRY
including biophysical chemistry & molecular biology

Article

pubs.acs.org/biochemistry

Charge and Charge-Pair Mutations Alter the Rate of Assembly and Structural Properties of Apolipoprotein C-II Amyloid Fibrils

Yu Mao, Chai Lean Teoh, Shuo Yang, Courtney O. Zlatic, Zachary K. Rosenes, Paul R. Gooley, Geoffrey J. Howlett, and Michael D. W. Griffin*

Department of Biochemistry and Molecular Biology, Bio21 Molecular Science and Biotechnology Institute, University of Melbourne, Parkville, Victoria 3010, Australia

ABSTRACT: The misfolding, aggregation, and accumulation of proteins as amyloid fibrils is a defining characteristic of several debilitating diseases. Human apolipoprotein C-II (apoC-II) amyloid fibrils are representative of the fibrils formed by a number of plasma apolipoproteins implicated in amyloid-related disease. Previous structural analyses identified a buried charge pair between residues K30 and D69 within apoC-II amyloid fibrils. We have investigated the effects of amino acid substitutions of these residues on apoC-II fibril formation. Two point mutations of apoC-II, D69K and K30D, as well as a reversed ion-pair mutant containing both mutations (KDDK) were generated. Fibril formation by the double mutant, apoC-II KDDK, and apoC-II D69K was enhanced compared to that of wild-type (WT) apoC-II, while apoC-II K30D lacked the ability to form fibrils under standard conditions. Structural analyses showed that WT apoC-II, apoC-II D69K, and apoC-II KDDK fibrils have similar secondary structures and morphologies. Size distribution analyses revealed that apoC-II D69K fibrils have a broader range of fibril sizes while apoC-II KDDK fibrils showed an increased frequency of closed fibrillar loops. ApoC-II D69K fibrils exhibited reduced thioflavin T binding capacity compared to that of fibrils formed by WT apoC-II and apoC-II KDDK. These results indicate that specific charge and charge-pair mutations within apoC-II significantly alter the ability to form fibrils and that position 69 within apoC-II plays a key role in the rate-limiting step of apoC-II fibril formation.

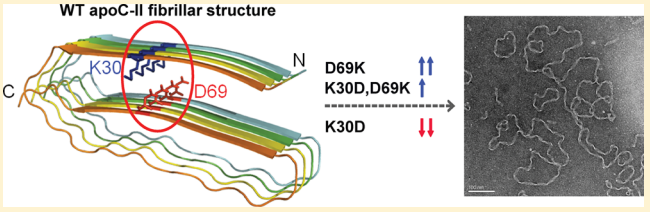

Amyloid fibrils accumulate during the course of several debilitating diseases, including Alzheimer's disease, Parkinson's disease, and type II diabetes. These fibrils are defined by their cross-β structure and ability to interact with the dyes thioflavin T (ThT) and Congo Red.[1] Several environmental conditions affect the ability of proteins to form amyloid fibrils, including the presence of lipids or lipid complexes, metal ions, glycosaminoglycans, proteins,[2] changes in temperature[3] ionic strength[4] and pH,[5,6] and exposure to interfaces[7,8] and oxidative agents.[9−11] Amyloid fibril formation by human apolipoprotein C-II (apoC-II) is representative of the ability of a number of plasma apolipoproteins to form fibrils and accumulate within the body in amyloid plaques. Immunohistochemistry of human coronary artery plaques shows colocalization of apoC-II with serum amyloid P, a universal marker for amyloid deposits.[12] ApoC-II fibrils, as well as Aβ fibrils, activate macrophage inflammatory responses via the CD36 receptor, leading to an increase in the level of production of reactive oxygen species.[13] Activation of macrophages is associated with foam cell formation, an early event in the development of atherosclerosis.

ApoC-II adopts a predominantly α-helical conformation in complex with lipid, and the structure of the protein in complex with sodium dodecyl sulfate and dodecyl phosphocholine micelles has been determined.[14,15] In each case, well-defined helices were observed for residues 15−39 and 63−77. These helices are separated by more flexible structure, and no long-range nuclear Overhauser effects were observed to suggest these helices interact. Conversely, lipid-free apoC-II readily forms amyloid fibrils that are enriched in β-structure, under quiescent conditions *in vitro*.[16−19] A three-layer, "G-like" β-strand−loop−β-strand model has been proposed for apoC-II amyloid fibrils.[20] This structural model indicates a buried charge pair involving K30 and D69 within the cross-β core of the fibrils, where the side chain of the sole tryptophan, W26, is located in the interior of the fibril structure. The two β-strands encompassing residues 20−36 and 58−74 are in parallel register within monomer units and also parallel within the cross-β sheets. Fully solvated all-atom molecular dynamics (MD) simulations showed that the model contained a stable cross-β core with a flexible connecting loop devoid of persistent secondary structure.[20] The time course of the MD simulations revealed that charge clusters in the fibril rearrange to minimize the effects of same-charge interactions inherent in parallel in-register models.[20] The proposed model provides a scaffold for examining how specific amino acid residues affect fibril formation.

This work explores the potential importance of buried charged-pair residues K30 and D69 within apoC-II fibrils. Three mutants of apoC-II, D69K, K30D, and double mutant K30D/D69K (KDDK), were generated. Kinetic and structural

Received: November 24, 2014
Revised: January 19, 2015
Published: January 21, 2015

DOI: 10.1021/bi5014535
Biochemistry 2015, 54, 1421−1428

analyses of these mutants showed that positions 30 and 69 within apoC-II exert significant effects on the ability of apoC-II to form fibrils.

MATERIALS AND METHODS

Expression, Mutagenesis, and Purification of ApoC-II. ApoC-II D69K, apoC-II K30D, and apoC-II KDDK were constructed by the QuikChange method using the pET-11a expression vector containing human apoC-II cDNA[21] according to the manufacturer's protocol (Agilent Technologies). Mutations were verified by DNA sequencing (Applied Genetic Diagnostics, Victoria, Australia). Wild-type (WT) and mutated apoC-II expression vectors were isolated and purified by Miniprep (Qiagen Inc.) and transformed into *Escherichia coli* BL21(DE3) cells for expression and purification as described previously.[21] The molecular masses of WT apoC-II and mutant apoC-II preparations were confirmed using an ESI-TOF 6220 mass spectrometer (Agilent Technologies). Purified apoC-II and apoC-II variants were stored as 30−40 mg/mL stocks at −20 °C in 5 M GuHCl and 10 mM Tris-HCl (pH 8.0).

Fibril Formation. Fibril formation was initiated by dilution of protein stocks (30−40 mg/mL) to 0.3 mg/mL (33.6 μM) protein in refolding buffer [100 mM sodium phosphate buffer (pH 7.4)]. This step reduces the GuHCl concentration to levels where it has little effect on apoC-II fibril formation. Fibril formation was conducted at room temperature (22 °C) to allow for accurate estimation of fibril formation rates by all mutant apoC-II constructs in all assays. With the exception of samples used directly in circular dichroism (CD) spectroscopy, all fibril-forming experiments were conducted in the presence of 0.1% sodium azide to prevent microbial contamination.

Thioflavin T Fluorescence Assays. Thioflavin T (ThT) is a histochemical reagent commonly used to monitor amyloid fibril formation, both *in vitro* and *in vivo*,[22,23] and was purchased from Sigma (St. Louis, MO). At selected time points after initialization of fibril formation, 20 μL aliquots of the incubation mixture were removed and mixed in a 96-well microtiter plate with 230 μL of ThT and 100 mM sodium phosphate buffer (pH 7.4) to a final ThT concentration of 10 μM. Fluorescence intensities were measured using an f_{max} fluorescence plate reader (Molecular Devices) with excitation and emission filters of 444 and 485 nm, respectively. Measurements were taken in duplicate and corrected by subtracting the zero hour time point reading. ThT fluorescence intensity time courses for apoC-II samples were fit to a sigmoidal Hill plot (eq 1) to obtain estimates for the half-time (t_{50}) for fibril formation:

$$S = \frac{S_{max} t^n}{t_{50}{}^n + t^n} \quad (1)$$

where S is the intensity of ThT fluorescence, S_{max} is the maximal change in ThT fluorescence, n is a scaling factor, t is the time in hours, and t_{50} is the time to the half-maximal fluorescence change.

Pelleting Assays. Freshly refolded samples were incubated at 22 °C. At selected time points, sample aliquots (180 μL) were centrifuged at 100000 rpm (350000*g*) for 30 min using an OptimaMax centrifuge and TL-100 rotor (Beckman Coulter Inc.). The supernatant was then carefully removed and diluted with an equal volume of 5 M GuHCl (pH 8) to halt fibril formation. The amount of protein present in the supernatant fractions (nonsedimenting protein) and the total amount of protein present in the samples prior to centrifugation were determined using the intrinsic fluorescence of tryptophan in the protein as described previously.[8] Fluorescence emission spectra were recorded using a Cary Eclipse fluorescence spectrometer (Agilent Technologies) at an excitation wavelength of 295 nm. Protein concentrations were determined from the emission intensity at 365 nm using a calibration curve constructed using known concentrations of apoC-II in the same buffer. The amount of protein pelleted was determined as the difference in protein concentration between the supernatant fractions and the uncentrifuged sample.

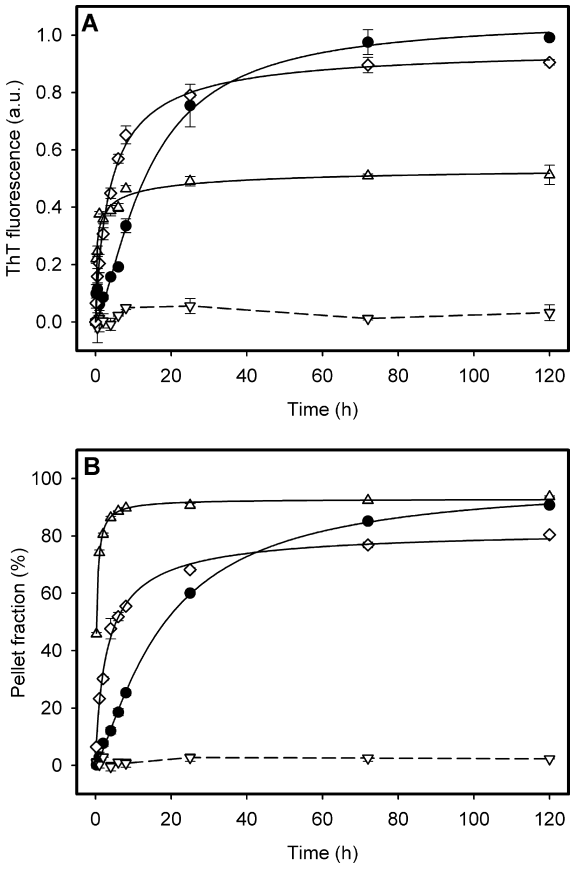

Figure 1. ApoC-II fibril formation monitored by (A) a ThT fluorescence assay and (B) a pelleting assay. Fibril formation by WT apoC-II (●), apoC-II D69K (△), apoC-II K30D (▽), and apoC-II KDDK (◇) was initiated by incubation of samples at 0.3 mg/mL in 100 mM sodium phosphate buffer (pH 7.4) at 22 °C. Error bars represent the standard deviation derived from duplicate measurements. Solid lines represent the best fits to the data using eq 1.

Circular Dichroism Spectroscopy. Far-UV CD experiments were performed using an Aviv model 410 SF CD spectrometer (Aviv Biomedical Inc.) at 20 °C with a 0.5 mm path length quartz cuvette. Samples of 0.3 mg/mL were prepared by diluting apoC-II stock solutions into 100 mM sodium phosphate buffer (pH 7.4). CD spectra were recorded at a spectral bandwidth of 1 nm, from 195 to 250 nm with an interval of 0.5 nm, and an averaging time of 4 s. Spectra were corrected using data obtained for a reference solution lacking apoC-II.

Transmission Electron Microscopy. Carbon-coated copper grids (300 mesh) were glow discharged for 10 s. Samples of apoC-II fibrils were diluted to 0.1 mg/mL with Milli-Q water and placed on a grid. After 1 min, the excess solution was wicked away with filter paper. The grids were

DOI: 10.1021/bi5014535
Biochemistry 2015, 54, 1421−1428

subsequently stained twice with 5 μL of 2% potassium phosphotungstate for 10 s followed by blot drying. An FEI Tecnai G2 TF30 instrument (FEI) operating at 200 kV was used to examine the grids, and images were taken digitally using a Gatan US1000 2kX2k CCD camera (Gatan Inc.).

Sedimentation Velocity Analysis. ApoC-II samples (0.3 mg/mL) were incubated in 100 mM sodium phosphate refolding buffer (pH 7.4) at 22 °C for 168 h. Sample (380 μL) and buffer reference (400 μL) solutions were loaded into 12 mm double-sector cells with quartz windows and centrifuged at 8000 rpm and 20 °C using a Beckman XL-I analytical ultracentrifuge and An-60Ti four-hole rotor (Beckman Coulter Inc.). Radial absorbance data were collected at a wavelength of 280 nm in continuous scanning mode. Sedimentation velocity profiles of apoC-II fibrils were analyzed with SEDFIT using a continuous sedimentation coefficient [$c(s)$] model,[24] assuming a wormlike chain model for noninteracting fibrils and a relation between the sedimentation coefficient and fibril molecular weight described previously.[17] Because of the broad size distribution of apoC-II fibrils, Tikhonov–Phillips regularization[25] was used with p = 0.95 and 250 sedimentation coefficient increments. The baseline absorbance was floated, and the meniscus position was fixed.

ThT Binding Assay. A centrifugation study combined with UV–vis absorbance scans was used to determine the direct binding of ThT to fibrils. ApoC-II sample aliquots (200 μL) were centrifuged at 100000 rpm for 30 min using an OptimaMax centrifuge and TL-100 rotor (Beckman Coulter Inc.). The pellet fractions were resuspended in 100 μL of 5 M GuHCl (pH 8) for 4 h to dissociate fibrils into monomers. The pellet fractions treated with GuHCl were then scanned using a DU800 UV–vis spectrometer recording the absorbance over a range of wavelengths (230–450 nm) using 1 nm intervals. The concentration of ThT in the pellet fractions, corresponding to the amount of ThT bound to the fibrils, was determined using a calibration curve constructed using known ThT concentrations in 5 M GuHCl. The amount of protein in the pellet fractions was determined using the absorbance measured at 280 nm.

Table 1. Parameters of ThT and Pelleting Assays for ApoC-II Fibril Formation

	ThT assay		pelleting assay	
sample[a]	S_{max} (au)[b]	t_{50} (h)[b]	nonsedimenting %[c]	t_{50} (h)[c]
WT apoC-II	1.06	14.0	9.3	18.1
apoC-II D69K	0.56	0.49	6.3	0.25
apoC-II K30D	–	–	97.7	–
apoC-II KDDK	0.96	4.1	19.6	3.3

[a]Samples (0.3 mg/mL) were incubated in 100 mM sodium phosphate buffer (pH 7.4) at 22 °C for 120 h. [b]Values derived from ThT assays for the maximal ThT fluorescence (S_{max}) and t_{50} were determined by fitting the data in Figure 1A to a Hill equation (eq 1). [c]Values derived from pelleting assays for nonsedimenting apoC-II refer to the proportion of protein remaining in the supernatant fraction at 120 h compared to the total amount of protein initially present, prior to centrifugation. t_{50} values were determined by fitting the data in Figure 1B to a Hill equation (eq 1).

RESULTS

Effects of Mutation on ApoC-II Fibril Formation. The ability of apoC-II variants (WT, D69K, K30D, and KDDK) to form fibrils was evaluated by ThT fluorescence and pelleting assays. Samples of WT apoC-II, apoC-II D69K, apoC-II K30D, and apoC-II KDDK were diluted into refolding buffer at pH 7.4 to a final concentration of 0.3 mg/mL and incubated at room temperature. The change in ThT fluorescence intensity for each sample was monitored as an indicator of fibril formation (Figure 1A). The data were fit empirically to the Hill equation (solid lines) to obtain estimates for the maximal ThT fluorescence and time to reach half-maximal fibril formation (t_{50}). WT apoC-II showed a time-dependent increase to a plateau

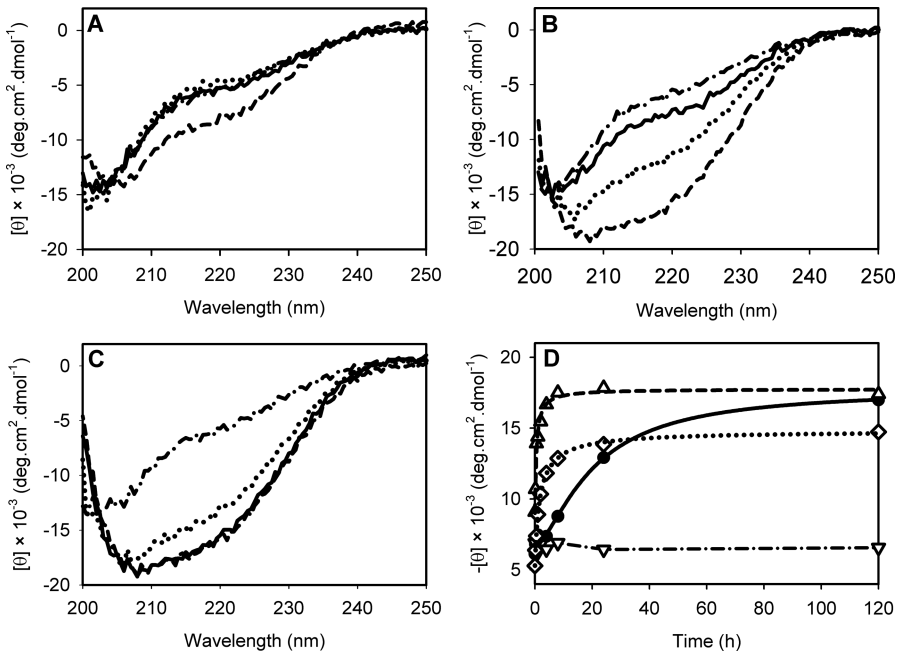

Figure 2. CD spectra of apoC-II samples at different time points during fibril formation. Mean residue ellipticities [θ] of WT apoC-II (—), apoC-II D69K (– – –), apoC-II K30D (–·–), and apoC-II KDDK (···) were recorded at (A) 0, (B) 8, and (C) 120 h. (D) Change in [θ] at 215 nm for WT apoC-II (●), apoC-II D69K (△), apoC-II K30D (▽), and apoC-II KDDK (◇) vs incubation time.

DOI: 10.1021/bi5014535
Biochemistry 2015, 54, 1421–1428

level of ThT fluorescence intensity with an estimated half-time for fibril formation of 14.0 h (Table 1). Under the same conditions, the double mutant with ion-pair residues reversed, apoC-II KDDK, formed fibrils more rapidly with a half-time of approximately 4.1 h. For the single-point mutation at position 30, apoC-II K30D, there was no significant change in ThT fluorescence, indicating no significant fibril formation. In contrast, for the single-site mutant at position 69, apoC-II D69K, there was a very rapid rise in ThT fluorescence (t_{50} = 0.49 h), reaching a plateau level after 24 h.

A pelleting assay, monitoring the depletion of apoC-II monomers in the supernatant following high-speed centrifugation, provided a more direct way to determine the extent of protein aggregation over time. WT apoC-II showed a sigmoidal increase in the proportion of protein pelleted over 120 h (Figure 1B), characterized by a t_{50} of 18.1 h (Table 1) similar to the value obtained using the ThT assay (Table 1). The kinetic pattern for apoC-II KDDK fibrils obtained using the pelleting assay also gives good agreement with the results of the ThT assay. The pelleting assay indicated 19.6% of apoC-II KDDK remained in the supernatant after 120 h, compared to 9.3% for WT apoC-II (Table 1). This result indicates less complete fibril formation by apoC-II KDDK, consistent with the lower plateau level of ThT fluorescence observed for apoC-II KDDK compared with that of WT apoC-II (Figure 1A and Table 1). For apoC-II K30D, the pelleting assay supports the observation from the ThT assay that no significant aggregation occurred during the incubation time of 120 h. ApoC-II D69K showed rapid fibril formation, with a t_{50} of 0.25 h, consistent with the ThT fluorescence measurements; 6.3% of apoC-II D69K remained in the supernatant after 120 h, indicating that the amount of fibrils formed was very similar to that of WT apoC-II. Thus, the reduced ThT fluorescence yield in the presence of apoC-II D69K fibrils with respect to WT apoC-II fibrils (Figure 1A and Table 1) may be due to a reduced level of binding of ThT to the mature apoC-II D69K fibrils.

Secondary Structure of Mutant ApoC-II during Fibril Formation. Far-UV CD spectroscopy was used to monitor the changes in the secondary structure of apoC-II mutants during fibril formation (Figure 2). The CD spectra revealed that freshly refolded WT apoC-II, apoC-II K30D, and apoC-II KDDK were largely unstructured. In contrast, apoC-II D69K showed a small increase in negative ellipticity above 205 nm suggesting some secondary structure. This observation is most likely caused by partial fibril formation due to the high rate of fibril formation by apoC-II D69K and the time taken for spectral acquisition. After 8 h, the apoC-II D69K sample showed the largest change in secondary structure, followed by the apoC-II KDDK sample. WT apoC-II showed a minor change compared with the freshly refolded state, while the apoC-II K30D sample did not show any significant spectral changes. After incubation for 120 h, the spectra for WT apoC-II and apoC-II D69K samples were similar, indicating the acquisition of similar secondary structure content. Spectra recorded at 120 h for the apoC-II KDDK sample showed an increase in the level of secondary structure, but it was smaller than that of the WT apoC-II or apoC-II D69K sample. In combination with the results of the pelleting assay (Table 1), the spectrum of apoC-II KDDK suggested that there was a mixture of fibrils and free monomers in the sample. For apoC-II K30D, the spectrum remained characteristic of random coil over 120 h without any change. This result further supports the conclusion that apoC-II K30D does not form fibrils under these conditions. Figure 2D shows time courses for mean residue ellipticity at 215 nm. The changes in ellipticity at this wavelength are an indicator of increased secondary structure content associated with amyloid fibril formation and are consistent with the time courses for fibril formation estimated by the ThT and pelleting assays (Figure 1).

Morphologies of Amyloid Fibrils Formed by Mutant ApoC-II Derivatives. The morphologies of amyloid fibrils formed by WT apoC-II, apoC-II D69K, and apoC-II KDDK after incubation for 120 h were investigated by transmission electron microscopy (TEM). The fibrils formed by WT apoC-II appeared as twisted ribbon fibrils of indefinite length that tangled together (Figure 3A), consistent with previous

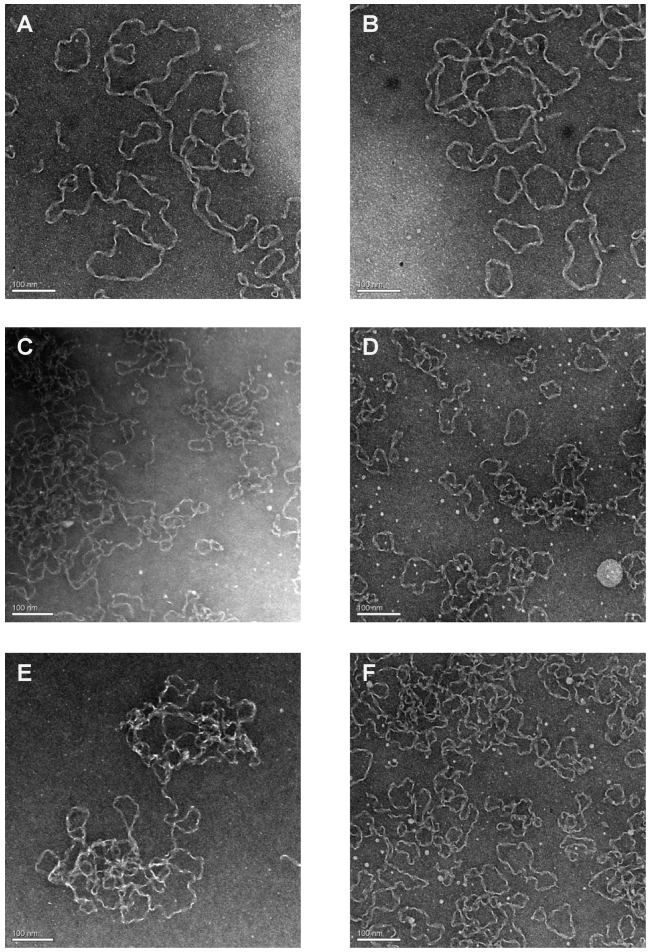

Figure 3. TEM images of apoC-II amyloid fibrils. Fibrils were formed by incubation of 0.3 mg/mL apoC-II variants in 100 mM sodium phosphate buffer (pH 7.4) at 22 °C for 120 h. Panels A, C, and E present TEM images of fibrils formed by WT apoC-II, apoC-II D69K, and apoC-II KDDK, respectively. Mature fibrils were subjected to centrifugation at 50000 rpm (47500*g*) for 8 min, and the slowly sedimenting fractions in the supernatant were collected. Panels B, D, and F present TEM images of the slowly sedimenting fractions of amyloid fibrils formed by WT apoC-II, apoC-II D69K, and apoC-II KDDK, respectively. Scale bars for TEM images represent 100 nm.

observations.[21] Fibrils formed by apoC-II D69K (Figure 3C) or apoC-II KDDK (Figure 3E) showed morphology similar to that of WT apoC-II fibrils. These unbranching fibrils appeared as either twisted, long linear fibrils or smaller closed loop fibrils.

Sedimentation Velocity Analyses of Fibrils Formed by ApoC-II Variants. Sedimentation velocity analysis was performed to determine the size distributions of mutant apoC-II

DOI: 10.1021/bi5014535
Biochemistry 2015, 54, 1421−1428

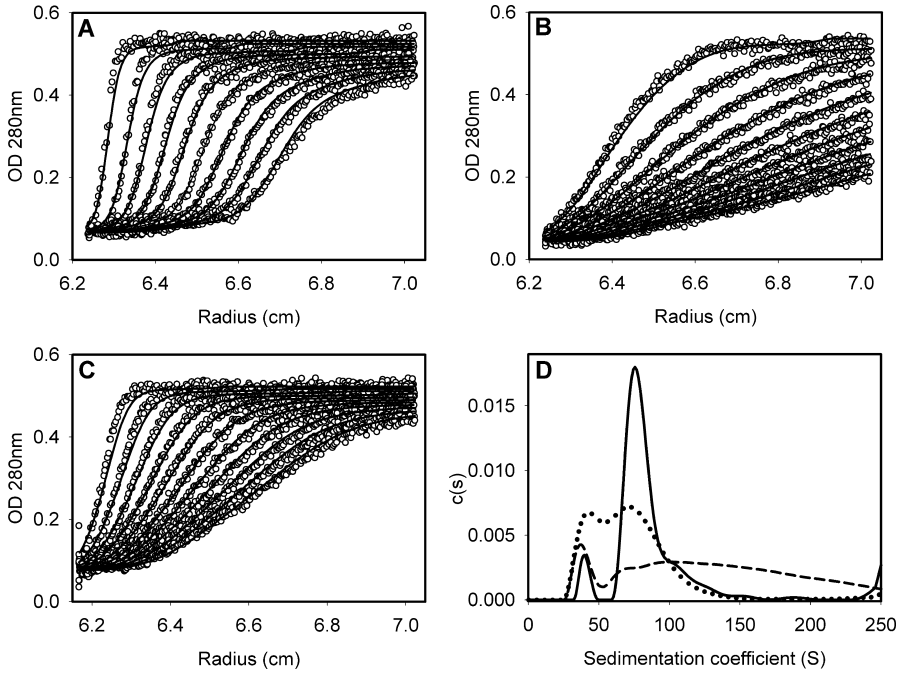

Figure 4. Sedimentation velocity analyses of fibrils formed by apoC-II variants. ApoC-II samples (0.3 mg/mL) were incubated in 100 mM sodium phosphate refolding buffer (pH 7.4) at 22 °C for 168 h. Raw sedimentation velocity data (○) are overlaid with fits to a continuous sedimentation coefficient distribution [$c(s)$] model (—) for (A) WT apoC-II, (B) apoC-II D69K, and (C) apoC-II KDDK. Radial absorbance scans collected at approximately 22 min intervals during sedimentation are shown. (D) Continuous sedimentation coefficient distributions calculated for WT apoC-II (—), apoC-II D69K (– – –), and apoC-II KDDK (···).

fibrils (Figure 4). For WT apoC-II fibrils (Figure 4A), the pattern of the moving boundaries corresponds to the migration of large soluble fibrils, consistent with previous studies.[16] ApoC-II D69K fibrils (Figure 4B) showed a much faster sedimentation rate with little nonsedimenting material remaining in the supernatant. The sedimentation velocity scans for apoC-II KDDK (Figure 4C) indicated that the sedimentation rate was similar to that of WT apoC-II, although there was more nonsedimenting material in the sample. This latter observation is consistent with the results of the pelleting assay (Figure 1B and Table 1).

The sedimentation velocity profiles (Figure 4A–C) were fit to a $c(s)$ model, which takes into account the effect of both sedimentation and diffusion.[24] The size distribution for fibrils formed by these three apoC-II constructs varied (Figure 4D). The apparent sedimentation coefficient distribution for fibrils formed by WT apoC-II ranged from 20 to 150 S with two peaks. The minor peak (20–50 S) corresponds to a population of small and short fibrils with closed loops, and the major peak area (50–150 S) corresponds to a population of longer linear apoC-II fibrils.[18,21,26] In Figure 4D, the minor peak for the apoC-II D69K sample was similar in size to that of WT apoC-II. This result suggested that the amount of short fibrils formed by apoC-II D69K is similar to that for WT apoC-II. ApoC-II D69K fibrils showed a much broader distribution profile compared with that of fibrils of WT apoC-II, indicating a significant population of larger aggregates. In comparison with WT apoC-II fibrils, apoC-II KDDK showed a similar range of species, but the populations differ with an increase in the area corresponding to the short fibrils and a decrease in the magnitude of the peak corresponding to the long linear fibrils.

Previous studies[18,21,26] demonstrated that the fraction of fibrils sedimenting in the range of 20–50 S corresponds to short fibrils with closed loops. A centrifugation study combined with electron microscopy was used to explore the morphology of these short fibrils formed by apoC-II D69K and apoC-II KDDK. Under the centrifugation conditions used, larger fibrils (>50 S) sediment rapidly and accumulate in the pellet fraction, while fibrils with lower sedimentation coefficients (≤50 S) remain in the supernatant fraction.[26] The supernatant fractions were examined by TEM. The short fibrils (≤50 S) formed by apoC-II D69K (Figure 3D) or apoC-II KDDK (Figure 3F) have a high proportion of closed loops with morphologies similar to those of the short fibrils formed by WT apoC-II (Figure 3B). These observations indicate that the population of fibrils with sedimentation coefficients in the range of 20–50 S formed by the apoC-II variants corresponds to the presence of closed loops.

ThT Binding Studies. A comparison of binding of ThT to apoC-II fibrils was made using a centrifugation study combined with UV–vis absorbance measurements, where the amount of ThT bound to the fibrils was estimated by analysis of the pellet fractions. The spectra in Figure 5A show a major peak at 280 nm corresponding primarily to protein absorbance, while the smaller peak at 415 nm corresponds to ThT absorbance. The samples of WT apoC-II, apoC-II D69K, and apoC-II KDDK pellet fractions showed similar maximal absorbance at 280 nm, although the value of the apoC-II KDDK sample was slightly lower than those of the WT and apoC-II D69K samples, consistent with the pelleting assay (Figure 1B and Table 1), which showed less complete fibril formation by apoC-II KDDK. It is notable that the ThT absorbance at 410 nm for the apoC-II D69K sample was lower than in the samples for WT apoC-II and apoC-II KDDK, suggesting apoC-II D69K fibrils bound less ThT. This would account for the lower maximal ThT fluorescence yield attained by apoC-II D69K fibrils compared to that of fibrils formed by WT apoC-II or apoC-II KDDK in the ThT assay (Figure 1A and Table 1).

DOI: 10.1021/bi5014535
Biochemistry 2015, 54, 1421–1428

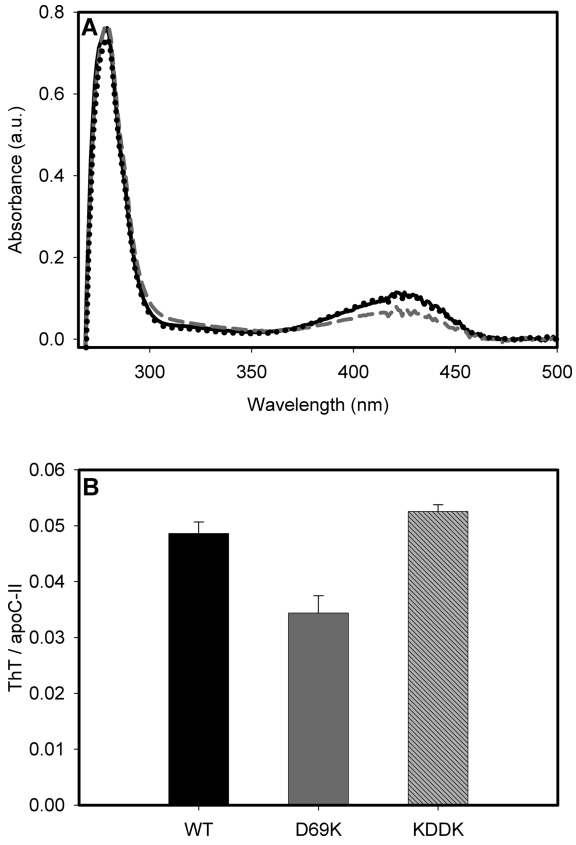

Figure 5. Analysis of binding of ThT to apoC-II fibrils. ApoC-II samples (0.3 mg/mL) were incubated in 100 mM sodium phosphate refolding buffer (pH 7.4) in the presence of 10 μM ThT at 22 °C for 168 h. (A) Absorbance scans for resuspended pellet fractions of apoC-II samples: WT apoC-II (—), apoC-II D69K (– – –), and apoC-II KDDK (···). (B) Ratios of ThT bound to apoC-II (moles of ThT per protein) for WT apoC-II (black bar), apoC-II D69K (gray bar), and apoC-II KDDK (diagonally lined bar). Error bars represent the standard deviation derived from duplicate measurements.

Figure 5B presents the binding ratio of ThT bound per apoC-II, determined using the amount of ThT present in the pellet fraction divided by the amount of protein present in the fibril pellet. These results showed that under the conditions used, fibrils formed by WT apoC-II or apoC-II KDDK have a similar ThT binding capacity (approximately 1 mol of ThT/20 mol of protein) while fibrils formed by apoC-II D69K have a lower ThT binding capacity (approximately 1 mol of ThT/30 mol of protein).

DISCUSSION

The "G-like" structural model for apoC-II fibrils depicted diagrammatically in Figure 6 is based on extensive physical studies, including fluorescence quenching studies, which localize the single tryptophan in apoC-II (W26) and K30 within the cross-β core.[20] Molecular dynamics simulations show that the energy cost of burying K30 within the core is at least partially offset by the formation of a charge-pair interaction between residues K30 and D69.[20] Our results for apoC-II KDDK show that reversing the orientation of the ion pair leads to an approximately 3–6-fold increase in the rate of fibril formation. The morphology of apoC-II KDDK fibrils is similar to that of WT apoC-II fibrils, albeit with an increased frequency of closed loop structures. These properties of apoC-II KDDK fibril formation are consistent with the ability to re-form the salt bridge. A similar

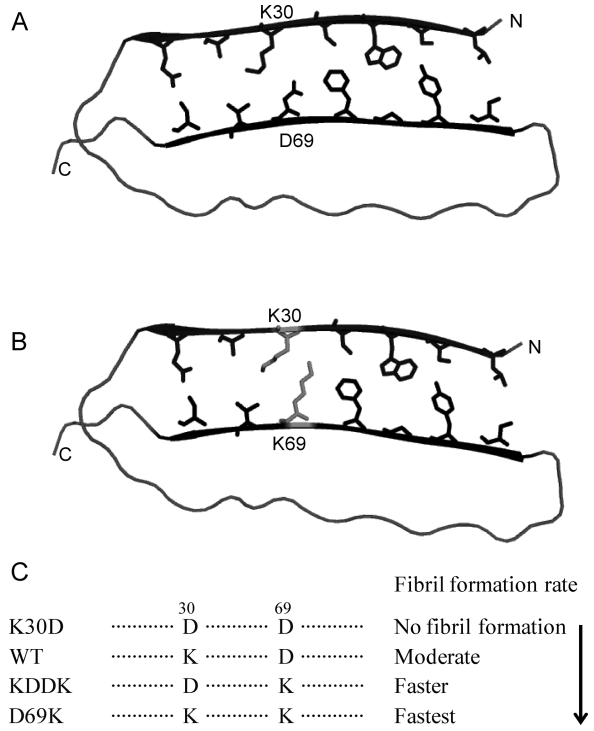

Figure 6. Structural models for amyloid fibrils formed by (A) WT apoC-II and (B) apoC-II D69K, derived from the apoC-II G-like fibril structure model.[20] Panel C illustrates the effects of substitutions of lysine and aspartate at positions 30 and 69 on the rate of fibril formation by apoC-II.

salt bridge involving D23 and K28 of Aβ has been observed, although this charge-pair interaction occurs in a loop region of Aβ fibrils.[27] Mutational studies with Aβ showed the complementary Aβ variant D23K/K28D also forms fibrils similar to WT Aβ fibrils, providing supporting evidence of the formation of a salt bridge between these residues.

Compared to apoC-II KDDK fibrils, single mutations in apoC-II at position 30 or 69 exert much larger effects on fibril formation. ApoC-II K30D did not form amyloid fibrils under standard fibril forming conditions. This observation is consistent with the need to stabilize charged residues at position 30 with oppositely charged residues elsewhere in the cross-β core. In contrast, the results from apoC-II D69K indicated a large increase in the rate of fibril formation of approximately 30–70-fold compared to that of WT apoC-II. These findings suggest that charge-pair formation is not an absolute requirement for fibril formation and that other factors are involved.

While the overall morphology of apoC-II D69K fibrils was similar to that of WT fibrils, there were significant differences in the ThT fluorescence and size distribution of these fibrils. Our results suggest that the lower ThT fluorescence observed for apoC-II D69K fibrils is due to a reduction in the level of binding of ThT. The positively charged benzothiazole moiety of ThT is considered to interact with negatively charged amino acid side chains leading to strong binding and enhanced ThT fluorescence.[28] Thus, the weakened ability of apoC-II D69K fibrils to bind ThT may be due to the overall reduction in net negative charge of these fibrils compared with that of WT apoC-II. It is also possible that the positive charge introduced by the D69K mutation produces direct electrostatic repulsion with the positive charge of the ThT molecule. Alternatively, subtle changes to the fibril structure induced by the mutation

DOI: 10.1021/bi5014535
Biochemistry 2015, 54, 1421–1428

may sterically alter the ThT binding site, thereby reducing the binding affinity. The size distribution of apoC-II D69K fibrils indicates an increase in the average size of the aggregates with respect to the size of WT apoC-II fibrils. This may be due to lateral association of fibrils, caused by alterations to the charge distribution or surface structure of the fibrils. It is also possible that the length of the fibrils is increased, possibly because of a change in the rate of fibril elongation.[18,26]

A consequence of the apoC-II D69K mutation is the placement of two lysine residues within the core of the cross-β structure (Figure 6). There are precedents for the presence of buried lysine residues within the core of protein structures.[29−31] These buried residues remain neutral with depressed pK_a values under conditions where the protein remains functional. In the case of apoC-II D69K, the long side chains of K30 and K69 may have sufficient flexibility to rearrange into energetically favored conformations resulting in delocalization of charge effects. In addition, the replacement of an aspartate residue with lysine at position 69 significantly increases the methylene content of the side chain, thereby possibly enhancing hydrophobic interactions and increasing the stability of the cross-β core within apoC-II fibrils.

Position 69 is present in an amyloidogenic region of apoC-II. This region spans residues 56−76 and shows strong protection from H/D exchange in mature fibrils. Isolated peptides composed of residues 56−76 or 60−70 of apoC-II retain the ability to form fibrils.[32] Changes in hydrophobicity within this region arising from the oxidation of M60 or the M60N substitution lead to significant inhibition of fibril formation.[10] We propose that the aspartate residue at position 69 in WT apoC-II plays an inhibitory role in apoC-II fibril formation such that loss of the negative charge at position 69, as occurs in apoC-II D69K and apoC-II KDDK, significantly increases the rate of fibril formation (Figure 6). An unfavorable effect of aspartate on the stability of β-sheet formation within an immunoglobulin-type domain has been reported.[33] Our proposal is consistent with previous studies indicating fibril formation by apoC-II is more rapid at low pH[34] where carboxyl groups become protonated and lose their negative charge. According to current models for apoC-II fibril formation, the effects of a negative charge at position 69 could be exerted at the level of the initial formation of an oligomeric nucleus required for fibril assembly or in the folding of the monomer into a fibril competent assembly unit and subsequent fibril elongation.[18,26]

AUTHOR INFORMATION

Corresponding Author

*Department of Biochemistry and Molecular Biology, Bio21 Molecular Science and Biotechnology Institute, University of Melbourne, 30 Flemington Rd., Parkville, Victoria 3010, Australia. Telephone: 61-3-9035-4233. Fax: 61-3-9348-1421. E-mail: mgriffin@unimelb.edu.au.

Funding

This work was supported by the Australian Research Council (Projects DP0877800 and DP110103528). M.D.W.G. is the recipient of the C. R. Roper Fellowship and an Australian Research Council Future Fellowship (Project FT140100544).

Notes

The authors declare no competing financial interest.

ACKNOWLEDGMENTS

We thank Dr. Yee-Foong Mok for helpful suggestions during the preparation of the manuscript.

ABBREVIATIONS

apo, apolipoprotein; CD, circular dichroism; TEM, transmission electron microscopy; ThT, thioflavin T; WT, wild type.

REFERENCES

(1) Sipe, J. D., and Cohen, A. S. (2000) Review: History of the amyloid fibril. *J. Struct. Biol. 130*, 88−98.

(2) Alexandrescu, A. T. (2005) Amyloid accomplices and enforcers. *Protein Sci. 14*, 1−12.

(3) Azuaga, A. I., Dobson, C. M., Mateo, P. L., and Conejero-Lara, F. (2002) Unfolding and aggregation during the thermal denaturation of streptokinase. *Eur. J. Biochem. 269*, 4121−4133.

(4) Gosal, W. S., Morten, I. J., Hewitt, E. W., Smith, D. A., Thomson, N. H., and Radford, S. E. (2005) Competing pathways determine fibril morphology in the self-assembly of β2-microglobulin into amyloid. *J. Mol. Biol. 351*, 850−864.

(5) Carneiro, F. A., Ferradosa, A. S., and Da Poian, A. T. (2001) Low pH-induced conformational changes in vesicular stomatitis virus glycoprotein involve dramatic structure reorganization. *J. Biol. Chem. 276*, 62−67.

(6) Giri, K., Bhattacharyya, N. P., and Basak, S. (2007) pH-dependent self-assembly of polyalanine peptides. *Biophys. J. 92*, 293−302.

(7) Zhao, H., Tuominen, E. K., and Kinnunen, P. K. (2004) Formation of amyloid fibers triggered by phosphatidylserine-containing membranes. *Biochemistry 43*, 10302−10307.

(8) Griffin, M. D., Mok, M. L., Wilson, L. M., Pham, C. L., Waddington, L. J., Perugini, M. A., and Howlett, G. J. (2008) Phospholipid interaction induces molecular-level polymorphism in apolipoprotein C-II amyloid fibrils via alternative assembly pathways. *J. Mol. Biol. 375*, 240−256.

(9) Stewart, C. R., Tseng, A. A., Mok, Y. F., Staples, M. K., Schiesser, C. H., Lawrence, L. J., Varghese, J. N., Moore, K. J., and Howlett, G. J. (2005) Oxidation of low-density lipoproteins induces amyloid-like structures that are recognized by macrophages. *Biochemistry 44*, 9108−9116.

(10) Binger, K. J., Griffin, M. D., and Howlett, G. J. (2008) Methionine oxidation inhibits assembly and promotes disassembly of apolipoprotein C-II amyloid fibrils. *Biochemistry 47*, 10208−10217.

(11) Wong, Y. Q., Binger, K. J., Howlett, G. J., and Griffin, M. D. (2010) Methionine oxidation induces amyloid fibril formation by full-length apolipoprotein A-I. *Proc. Natl. Acad. Sci. U.S.A. 107*, 1977−1982.

(12) Stewart, C. R., Haw, A., III, Lopez, R., McDonald, T. O., Callaghan, J. M., McConville, M. J., Moore, K. J., Howlett, G. J., and O'Brien, K. D. (2007) Serum amyloid P colocalizes with apolipoproteins in human atheroma: Functional implications. *J. Lipid Res. 48*, 2162−2171.

(13) Medeiros, L. A., Khan, T., El Khoury, J. B., Pham, C. L., Hatters, D. M., Howlett, G. J., Lopez, R., O'Brien, K. D., and Moore, K. J. (2004) Fibrillar amyloid protein present in atheroma activates CD36 signal transduction. *J. Biol. Chem. 279*, 10643−10648.

(14) MacRaild, C. A., Hatters, D. M., Howlett, G. J., and Gooley, P. R. (2001) NMR structure of human apolipoprotein C-II in the presence of sodium dodecyl sulfate. *Biochemistry 40*, 5414−5421.

(15) MacRaild, C. A., Howlett, G. J., and Gooley, P. R. (2004) The structure and interactions of human apolipoprotein C-II in dodecyl phosphocholine. *Biochemistry 43*, 8084−8093.

(16) MacRaild, C. A., Stewart, C. R., Mok, Y. F., Gunzburg, M. J., Perugini, M. A., Lawrence, L. J., Tirtaatmadja, V., Cooper-White, J. J., and Howlett, G. J. (2004) Non-fibrillar components of amyloid deposits mediate the self-association and tangling of amyloid fibrils. *J. Biol. Chem. 279*, 21038−21045.

DOI: 10.1021/bi5014535
Biochemistry 2015, 54, 1421−1428

(17) MacRaild, C. A., Hatters, D. M., Lawrence, L. J., and Howlett, G. J. (2003) Sedimentation velocity analysis of flexible macromolecules: Self-association and tangling of amyloid fibrils. *Biophys. J. 84*, 2562−2569.
(18) Binger, K. J., Pham, C. L., Wilson, L. M., Bailey, M. F., Lawrence, L. J., Schuck, P., and Howlett, G. J. (2008) Apolipoprotein C-II amyloid fibrils assemble via a reversible pathway that includes fibril breaking and rejoining. *J. Mol. Biol. 376*, 1116−1129.
(19) Mok, Y. F., Ryan, T. M., Yang, S., Hatters, D. M., Howlett, G. J., and Griffin, M. D. (2011) Sedimentation velocity analysis of amyloid oligomers and fibrils using fluorescence detection. *Methods 54*, 67−75.
(20) Teoh, C. L., Pham, C. L., Todorova, N., Hung, A., Lincoln, C. N., Lees, E., Lam, Y. H., Binger, K. J., Thomson, N. H., Radford, S. E., Smith, T. A., Muller, S. A., Engel, A., Griffin, M. D., Yarovsky, I., Gooley, P. R., and Howlett, G. J. (2011) A Structural Model for Apolipoprotein C-II Amyloid Fibrils: Experimental Characterization and Molecular Dynamics Simulations. *J. Mol. Biol. 405*, 1246−1266.
(21) Hatters, D. M., MacPhee, C. E., Lawrence, L. J., Sawyer, W. H., and Howlett, G. J. (2000) Human apolipoprotein C-II forms twisted amyloid ribbons and closed loops. *Biochemistry 39*, 8276−8283.
(22) Saeed, S. M., and Fine, G. (1967) Thioflavin-T for amyloid detection. *Am. J. Clin. Pathol. 47*, 588−593.
(23) Naiki, H., Higuchi, K., Hosokawa, M., and Takeda, T. (1989) Fluorometric determination of amyloid fibrils in vitro using the fluorescent dye, thioflavin T1. *Anal. Biochem. 177*, 244−249.
(24) Schuck, P. (2000) Size-distribution analysis of macromolecules by sedimentation velocity ultracentrifugation and Lamm equation modeling. *Biophys. J. 78*, 1606−1619.
(25) Schuck, P., and Rossmanith, P. (2000) Determination of the sedimentation coefficient distribution by least-squares boundary modeling. *Biopolymers 54*, 328−341.
(26) Yang, S., Griffin, M. D., Binger, K. J., Schuck, P., and Howlett, G. J. (2012) An equilibrium model for linear and closed-loop amyloid fibril formation. *J. Mol. Biol. 421*, 364−377.
(27) Petkova, A. T., Yau, W. M., and Tycko, R. (2006) Experimental constraints on quaternary structure in Alzheimer's β-amyloid fibrils. *Biochemistry 45*, 498−512.
(28) Kelenyi, G. (1967) On the histochemistry of azo group-free thiazole dyes. *J. Histochem. Cytochem. 15*, 172−180.
(29) Isom, D. G., Cannon, B. R., Castaneda, C. A., Robinson, A., and Garcia-Moreno, B. (2008) High tolerance for ionizable residues in the hydrophobic interior of proteins. *Proc. Natl. Acad. Sci. U.S.A. 105*, 17784−17788.
(30) Takayama, Y., Castaneda, C. A., Chimenti, M., Garcia-Moreno, B., and Iwahara, J. (2008) Direct evidence for deprotonation of a lysine side chain buried in the hydrophobic core of a protein. *J. Am. Chem. Soc. 130*, 6714−6715.
(31) Isom, D. G., Castaneda, C. A., Cannon, B. R., and Garcia-Moreno, B. (2011) Large shifts in pKa values of lysine residues buried inside a protein. *Proc. Natl. Acad. Sci. U.S.A. 108*, 5260−5265.
(32) Wilson, L. M., Mok, Y. F., Binger, K. J., Griffin, M. D., Mertens, H. D., Lin, F., Wade, J. D., Gooley, P. R., and Howlett, G. J. (2007) A structural core within apolipoprotein C-II amyloid fibrils identified using hydrogen exchange and proteolysis. *J. Mol. Biol. 366*, 1639−1651.
(33) Pokkuluri, P. R., Raffen, R., Dieckman, L., Boogaard, C., Stevens, F. J., and Schiffer, M. (2002) Increasing protein stability by polar surface residues: Domain-wide consequences of interactions within a loop. *Biophys. J. 82*, 391−398.
(34) Pham, C. (2006) The formation and structure of human apolipoprotein C-II fibrils. Ph.D. Thesis, University of Melbourne, Melbourne.

DOI: 10.1021/bi5014535
Biochemistry 2015, 54, 1421−1428